Effect of Interfacial Structure on Permeation Properties of Glassy Polymers

Sylvie Neyertz,* Anthony Douanne, and David Brown

Laboratoire Matériaux Organiques à Propriétés Spécifiques (LMOPS), UMR CNRS 5041, Université de Savoie, Bât. IUT, 73376 Le Bourget du Lac Cedex, France

Received July 6, 2005; Revised Manuscript Received September 23, 2005

ABSTRACT: Gas permeation has been studied in two fully atomistic molecular models of a glassy polyimide, which differ by their chain configurations and packing. The first polyimide system is an isotropic 56 025-atom bulk model of the amorphous phase while the second is a 141 100-atom model of an actual membrane. The preparation procedure of the membrane was based loosely on the experimental solvent-casting process. The membrane model exhibits density oscillations at the interfaces with chains being aligned and flattened parallel to it. The structuration persists throughout the membrane, and this leads to the gas diffusing in a slightly anisotropic way in the center of the membrane model. However, the diffusion coefficient obtained using either approximate analytical solutions or numerical solutions to the one-dimensional diffusion equation as well as a time-lag approach was found to be very similar to that in the bulk, which was evaluated from mean-square displacements, probability density distributions of displacement vector components, and the van Hove self-correlation function. Solubilities obtained from Widom's insertion technique and from the equilibrium density of gas within the matrix were in very good agreement for the membrane model. Despite a small drop in solubility in the region corresponding to the density peak of the polymer at the interface, the solubility coefficient also remained similar to that of the bulk. The changes in configurations and the high-density interface have thus little effect on the permeability of the gas used in this case.

1. Introduction

The relative rigidity of polyimide backbones combined with their potentially narrow free-volume distributions renders such macromolecules efficient dense membrane materials,[1] which can be used for gas-separation applications.[2,3] The relationships between chemical structures and permeabilities have been widely studied experimentally.[1−7] This has led to the development of empirical methods for prediction of gas permeation parameters.[8−14] Molecular dynamics (MD) simulations[15] have also attempted to link at the atomistic level the penetrant transport to the polyimide chemical structures, with the gas molecules being directly inserted into the matrices.[16−23]

Experimentally, the situation is more complicated as membrane pre-, post-, and processing[24,25] parameters are known to be of paramount importance: indeed, molecular weight,[26] residual solvent,[27] heating cycle,[28,29] casting conditions,[29] etc., have all been named as potentially influencing the physical properties of the polyimides.[24] Film thickness is also a key factor. Diffusivity and solubility of oxygen transport through dry Kapton membranes have been reported to increase along with the thickness of the samples.[30] In an intriguing work, it has been postulated that solubility and cohesion energy density increase in thinner glassy films.[31] Pinholes or defects in the thin layers are known to affect selectivity,[31] while defect-free layers are thought to provide greater size and shape discrimination, a property which is used in the design of asymmetric polyimide membranes.[32,33] It has also been suggested that free volume diffuses to a thin film surface,[34,35] which could explain thickness-related physical aging of thin polyimide films.[36,37]

This work was initiated following a combined experimental and MD simulation study on five closely related copolyimides for gas permeation applications.[38] Atomistic models of the polyimides in the bulk were in excellent agreement with the real systems in terms of densities, solubility parameters, *d* spacings, color indices, and free-volume fractions.[25,39,40] On the other hand, the calculated diffusion coefficients of He, O_2, or N_2 gas molecules were systematically higher than the experimentally measured ones,[38] despite the force fields being validated for both the matrices[40] and the gas molecules.[41,42] Several possible explanations for the disagreement between the models and the experiments have been put forward,[43] and this has led to a series of further simulations concerning specific features of such models. These studies are fundamental in nature and have general implications applicable to all glassy polymers and not just the polyimides under study here. In a first stage, it was shown that the microstructure and the permeation parameters in glassy polyimide models were independent of the simulation box size.[43] The second stage, presented here, deals with skin effects which, as explained above, are a well-known factor in these materials[3,31,33,44] A surface region of the membrane where the chains are either more or less ordered could significantly affect penetrant solubility and diffusion and maybe even act as the most important factor in the process of permeation.

Properties of polymers at interfaces have already been largely investigated using MD or Monte Carlo (MC) techniques.[45] From fairly early on, lattice MC simulations of polymer/vacuum or polymer/solid surfaces[46−49] showed that interfacial structure is clearly distinct from the central amorphous region. MD simulations of polymer melts confined between planar solid surfaces described the chains in the interfacial region as being flattened in the directions parallel to the wall.[50] The actual features were found to be dependent on a number of parameters such as the type of wall,[50] the chain

10.1021/ma051463y CCC: $30.25
Published on Web 10/27/2005

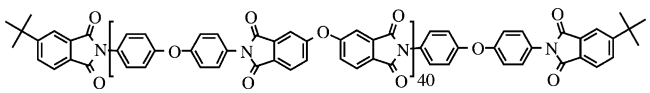

Figure 1. ODPA−ODA homopolyimide chain under study.

stiffness,[51,52] the slit thickness,[53] or functional end groups.[54] As far as glassy polymers are concerned, static model microstates of atactic polypropylene (PP) exposed to graphite surface[55] were analyzed, which led qualitatively to the same types of conclusions than for the polymer melts. The wall effect is enhanced, and the chains stiffen at decreasing temperatures.[49] Related works include the investigations of polymer−polymer interfaces (see e.g. refs 56−58), which have to deal with additional features such as polymer miscibility and interpenetration.[59] Also of interest are the simulations of free-standing thin films where the key issue is the local structure at the polymer/vacuum interfaces[60−62] as well as crystal surfaces.[63] As far as permeation is concerned, helium and neon permeation was probed in both rubbery and glassy polymethylene matrices confined between structureless planar graphite walls by changing the temperature, in an attempt to model hybrid organic−inorganic materials.[64]

The aim of the present work is to characterize the differences between a large 56 025-atom bulk periodic model of the amorphous core of a glassy polyimide membrane and that of an even larger 141 100-atom model of dimensions $\sim 110 \times 110 \times 160$ Å^3 containing actual surfaces. Since the selectivities associated with defect-free skin layers have been correlated with high polymer packing density in the skin layer,[33] the polyimide membrane model was confined between two impenetrable walls. This leads to high-density regions at the interface and is consistent with the fact that the actual polyimides were cast on a glass plate.[25] The matrix is the one used in the MD study of the box size dependence of gas transport in glassy polymers,[43] i.e., the ODPA−ODA homopolyimide (Figure 1). Here we make the same approximation of using purely repulsive Weeks−Chandler−Andersen (WCA) nonbonded interactions to speed up the MD calculations. The interaction parameters of the gas permeant have been adjusted to give the same solubility than that of the high-permeability helium (He) gas[6,65−67] when full Lennard-Jones (LJ) interactions are used.[43] Although penetrant diffusion in a glassy bulk polymer of this size has been studied using a coarse-grained method,[68] we are not aware of any fully atomistic model of this magnitude and periodic in two dimensions being created yet for glassy polyimide membranes.

2. Computational Details

All simulations were performed using either the *gmq* MD program[69] or its parallel form, *ddgmq*.[70] In the latter case, simulation boxes were decomposed either into $2 \times 2 \times 2 = 8$ or $4 \times 4 \times 4 = 64$ domains each.

2.1. Chemical Structures. The ODPA−ODA chains (Figure 1) were identical to those studied previously both experimentally[25,39] and by MD simulations.[40,43] Each chain had a total of 40 monomers and 2075 atoms. The gas probe was modeled as a single atom.

2.2. Potential. The force field for the polyimide used in this work has been described in detail elsewhere.[40,43] The total potentiel energy is given by the superposition of intramolecular bending, torsional and out-of-plane analytical functions, and the so-called "nonbonded" potentials, which are given below.

During the preparation phases of the dense matrices, the following Lennard-Jones form for the van der Waals potential energy, U_{LJ}, was used:

$$U_{LJ}(r) = 4\epsilon((\sigma/r)^{12} - (\sigma/r)^6) \tag{1}$$

with r being the distance between two atoms, ϵ the well depth of the potential, and σ the distance at which the potential is zero. However, as discussed before,[43] the use of such realistic nonbonded potentials is costly for MD simulations of large glassy systems. Consequently, we adopted the same approach as in our previous paper,[43] where the realistic potentials were used only in the preparation and relaxation phases of the polyimide matrices before switching for the production to the short-ranged repulsive WCA potential, U_{WCA}:

$$\begin{bmatrix} U_{WCA}(r) = 4\epsilon((\sigma/r)^{12} - (\sigma/r)^6) + \epsilon & \text{when } r \le 2^{1/6}\sigma \\ U_{WCA}(r) = 0 & \text{when } r > 2^{1/6}\sigma \end{bmatrix} \tag{2}$$

As far as He diffusion in polyimides is concerned, the WCA form has already proven to be a reasonable approximation for the LJ potential: the trajectories are similar, and the diffusion coefficient is almost the same.[43] This is possible since the glassy matrix is hardly modified (see later) and He is a weakly interacting gas. In the case of larger penetrants such as O_2 or N_2, which are expected to modify to some small extent the structure of the matrix,[6,65−67] or other glassy matrices, caution has to be exercised when using a purely repulsive potential approach.

Unlike diffusion,[43] we have earlier analyzed He solubility in a polyimide bulk with the realistic LJ form using Widom's test-particle insertion method.[40,43,72,73] However, permeation is governed by both diffusion and solubility, the latter being quite low for He in polyimides compared to other gas molecules.[6,65−67] Since the switch to a WCA potential reduces even more the penetrant solubility, we did not use the realistic parameters for helium derived from Lee et al.,[74] i.e., $\sigma = 2.6282$ Å and $\epsilon/k_B = 6.030$ K. Instead, the ϵ was kept the same than for He, but the value of σ was decreased to 1.88 Å. This new value gives a solubility coefficient for the penetrant, with the WCA form (eq 2), which is the same as that obtained with the LJ form (eq 1) and the Lee parameters for He, i.e., 0.06 cm^3 (STP) cm^{-3} bar^{-1},[43] the experimentally estimated value for He being 0.04 cm^3 (STP) cm^{-3} bar^{-1}.[38] This ensures that the solubility of the gas permeant in the membrane is comparable to that of the reference bulk system. Standard combination rules were used for most cross parameters,[43] the only exception being for the gas−gas interaction parameters: these were switched off completely so that it behaved ideally.

Electrostatic interactions were evaluated using the Coulombic potential, U_{coul}:

$$U_{coul}(r) = q_i q_j / 4\pi\epsilon_0 r \tag{3}$$

with q_i and q_j being the partial charges on atoms i and j, respectively, and ϵ_0 being the vacuum permittivity. In the bulk system,[40,43] the Ewald summation method was used.[75,76] However, in the larger membrane model, which is effectively periodic in two dimensions, the Ewald sum is difficult to implement[45] and becomes

totally prohibitive in terms of computational time. It thus has to be replaced by other methods[77] such as tree-based[78] or mesh-based[79−81] approaches. Here, a particle-mesh technique using an iterative solution of the Poisson equation was implemented.[82] As in the Ewald method, the technique separates the Coulombic interaction into two parts: a short-range term and a smoothly decaying long-range term. The short-range contribution is calculated directly as a sum of pair interactions in real space. The long-range term though is no longer calculated in reciprocal space using Fourier transforms but is handled in real space with a smooth projection of discrete point charges to a grid[83] followed by a multigrid approach.[84] The advantages of such a technique are (i) it becomes progressively more efficient than Ewald as system sizes increase, (ii) it can be parallelized within a domain decomposition approach, and (iii) it is equally applicable to periodic, partially periodic, or nonperiodic systems.[82]

2.3. Preparation of the Models. 2.3.1. System Sizes. It has been shown in the literature that the influence of an interface will extend *at least* over a distance spanning the average radius of gyration, $\langle S^2\rangle^{1/2}$, of the molecules under study.[47,48,50−52] This is certainly the lower limit since ranges of 1−3 $\langle S^2\rangle^{1/2}$ have been quoted, depending on the molecules under study.[49,55,60]

$\langle S^2\rangle^{1/2}$ for the ODPA−ODA chains was evaluated using a well-documented "hybrid PMC-MD single-chain sampling" approach, which allows for chain configurations characteristic of the equilibrium melt to be created at the required temperature.[40,43,85−91] Since the experimental glass-transition temperature of the ODPA−ODA polyimide is ∼520 K,[38] sampling[91] was carried out in the melt at 700 K for a total of 5 ns using U_{LJ} (eq 1) and U_{coul} (eq 3) as the nonbonded potentials. The resulting mean-square radii of gyration, $\langle S^2\rangle$, was 3410 ± 20 Å^2, i.e., $\langle S^2\rangle^{1/2} \sim 58.4$ Å. Interestingly, the same calculations carried out using either U_{LJ} (eq 1) or U_{WCA} (eq 2) on their own gave $\langle S^2\rangle^{1/2}$ equal to ∼62.3 and ∼62.0 Å, respectively, as well as distributions indistinguishable from those obtained using $U_{LJ} + U_{coul}$. As mentioned before,[43] this indicates that replacing the nonbonded $U_{LJ} + U_{coul}$ combination by the much faster U_{WCA} potential will not modify significantly the chain configurations.

To set up a cubic MD box with a side length of $\sim 2\langle S^2\rangle^{1/2}$, 68 ODPA−ODA 40-unit chains were found to be required, given that the experimental density at 300 K is 1368 kg m^{-3}.[40] Such a membrane model amounts to 141 100 atoms, and although larger systems would be better for ensuring a complete distinction between the surface layers and the bulk, computational limitations prohibit increasing the size significantly. For making comparisons with a periodic model of the bulk, the 56 025-atom ODPA−ODA matrix from our previous study[43] was used. In the remaining part of the paper, we will distinguish between both models by referring to them as the "membrane" and the "bulk" simulations, respectively.

2.3.2. The Membrane Model. The preparation of the membrane model was based loosely on the experimental solvent-casting process.[25] The latter involves preparing a 10% (w/w) solution of the polymer in *m*-cresol and casting it onto a clean glass plate. Solvent is subsequently removed through an appropriate heat treatment, and the film is peeled off the glass plate by immersion in water.

Step 1: As inserting and then removing explicit solvent molecules would have rendered the simulation too costly, the solvation procedure was instead mimicked by choosing an initial volume for the 68-chain simulation box corresponding to the density of a 10% (w/w) solution. Since solvent evaporation occurs mostly through the uppermost surface of a film, the basis vectors in the x and y direction were left at the value expected from the experimental ODPA−ODA density, i.e., $a = b \approx 115$ Å, while the basis vector in the z direction was increased to $c \approx 1500$ Å corresponding to the density of 1067 kg m^{-3}, i.e., that of an ideal (90% *m*-cresol/10% ODPA−ODA) mixture. The 68 chains were then generated independently using the hybrid PMC-MD single-chain sampling method (see section 2.3.1.) at 700 K with U_{WCA}. These chains were randomly reoriented and distributed in the solution simulation box. Excluded-volume was progressively introduced,[39,43] and the simulation was cooled to 300 K at a rate of −1 K ps^{-1} through loose coupling to a heat bath[92] with a coupling constant equal to 0.1 ps.

Step 2: The process of densification resulting from solvent evaporation was modeled by first adding an impenetrable wall on either side of the box in the z-direction of the "solvated" system in order to form the interfaces. The impenetrable wall consisted of a 10-layer tetrahedral diamond lattice arrangement of a total of 4200 atoms linked through flexible bonds and bond angles. For the bonds, a simple harmonic spring potential was used with an equilibrium distance of 4 Å and a force constant of 8.2 kg s^{-2}. For the bends, an harmonic potential in the cosine of the bond angle[39] was applied with an equilibrium angle of 109.47° and a force constant of 200 kJ mol^{-1}. The middle of the wall was placed on the periodic boundary in the z-direction so that, effectively, some layers appear at the upper end and some layers appear at the lower end of the polymer box due to the continued imposition of periodic boundary conditions, the wall being thick enough to prevent any interactions between polymer chains on either side at all subsequent stages. The resulting wall + polymer box had a basis vector $c \approx 1760$ Å in the z direction. The wall atoms nonbonded interactions were set to $\sigma_{ii} = 6.2$ Å and $\epsilon_{ii}/k_B = 119.8$ K to maintain the tetrahedral network and avoid any penetration by the polymer. Since the surface area of a film remains quasi-constant throughout the experimental solvent evaporation process, the model wall + polymer box was subsequently compressed by shrinking the length of the cell in the z direction, while rescaling the z-positions of all atoms at each time step in an affine manner, over 135 ps at 300 K and over 25 more ps at 700 K to ∼160 Å. During this period, the surface area in the $x-y$ plane was kept constant. The target box length was chosen to take into account the dimensions expected from the experimental pure ODPA−ODA density for the polymer and the length of the wall.

Step 3: Experimentally, once most of the solvent has been evaporated at ambient conditions, the membranes are heat-treated to remove residual solvent and to relax internal stresses. To take this step into account, a constant-volume (NVT) run of 3000 ps at 700 K with U_{WCA} was performed in order for the chains to relax locally. At this point, the full $U_{LJ} + U_{coul}$ nonbonded potentials were introduced. The LJ potential was truncated at 10 Å, and long-range corrections to the energy and the pressure were applied.[15] Parameters associated

with the lattice diffusion multigrid procedure for the calculation of the long-range electrostatic forces[82] were as follows: the β coefficient was set to 0.24 Å^{-1}, and the mesh spacing in the x, y, and z directions were respectively $h_x = 0.583$ Å, $h_y = 0.589$ Å, and $h_z = 0.655$ Å. Charges were interpolated onto the grid via a Gaussian charge spreading where every particle charge was distributed over the 64 closest grid points. The optimized value for the charge-spreading diffusion coefficient was $D' = 0.0578$ Å^2 per iteration, and the number of steps for the diffusion scheme was $N_t = 72$. As expected from the very large size of the model membrane, the change of nonbonded potentials typically increased the required simulation time by a factor of ~70.

In the subsequent NVT run at 700 K with the full potential switched on, the Lennard-Jones energy quickly settled, in ~20 ps, to a stable value. The Coulombic energy was also found to decay quite rapidly from approximately −360 J g^{-1} (of polymer) to −1100 J g^{-1} in the first 50 ps and then continued to slowly decrease, reaching a value of about −1110 J g^{-1} by 250 ps. The system was then cooled to 300 K and allowed to settle for 100 ps. At that temperature, the Coulombic energy only drifted from −1145.5 to −1145.2 J g^{-1} in 50 ps. Since the system is in the glassy state and the overhead of running the $U_{LJ} + U_{coul}$ nonbonded potential is extremely heavy, the equilibration procedure for the membrane matrix was deemed to be sufficient at that stage. The dimensions of the box were slightly readjusted to have the same density in the middle part of the polymer than in the corresponding pure bulk model. The final basis vectors were $a = 112$ Å, $b = 113$ Å, and $c = 158$ Å. The preparation procedure of the 27-chain bulk model has been described in detail previously.[43] Its final average density at 300 K and 1 bar was ~1378 kg m^{-3}.

2.3.3. Insertion of Gas Probes. As explained earlier, the $U_{LJ} + U_{coul}$ nonbonded potentials were replaced with the much faster U_{WCA}, thus allowing for far longer simulation times to be attained. The overall structure of the glassy matrices is hardly modified, and penetrant motion within the matrix is very similar.[43] On the other hand, there is a well-known caveat associated with the use of the purely repulsive WCA potential in that, to maintain the density, either the simulations have to be run at constant volume or a compensating (over)-pressure field has to be applied. In the bulk, running under NVT conditions poses no problem. For the membrane, the density of the polymer was maintained by keeping the 10-layer wall in place. To insert the gas probes into a "vacuum" either side of the polymer, the ϵ_{ij} cross parameter between the wall atoms belonging to the three layers neighboring the polymer on either side of the membrane and the gas probes was set to zero. In this way, the four middle layers of the wall were impenetrable to both polymer and gas, while the three wall layers closest to each wall/polymer interface were impenetrable to the polymer but invisible to the gas.

The next consideration is how many gas probes should be introduced into the systems. As discussed previously,[43] if one were to respect the experimental solubility and conditions, i.e., an externally imposed pressure of 3 bar at room temperature,[38] it would amount to less than four gas probes being inserted into the 56 025-atom bulk matrix. To both improve the statistics for the diffusion of the penetrants and remain consistent with respect to the solubility of He, we have in the past set the number of gas probes inserted into the polyimide matrix, n_p, and adjusted the external pressure, P, accordingly.[43] On the other hand, in simulating an actual membrane, we must calculate the amount of gas to insert into the space either side of the membrane given that, as in reality, we cannot control the uptake of gas by the polymer.

In atomistic simulations, the solubility S at a certain temperature T is usually estimated using Widom's test-particle insertion method and the change in potential energy ΔU associated with repeated insertions.[72,73] While sorption in glassy polymers is most often described by the "dual-mode model",[93,94] small and not very soluble penetrants such as He are found to follow well Henry's law; i.e., the solubility of dissolved gas is linearly proportional to the pressure. This infinite dilution limit of S can then be simply related to the probability of insertion for the gas into the polymer, p_{ip}, with k_B being the Boltzmann constant:

$$S \propto p_{ip} = \left\langle \exp\left(-\frac{\Delta U}{k_B T}\right)\right\rangle \tag{4}$$

Now, if one considers an actual interfacial system constituted of a polymer membrane of volume V_p with some free space for the gas phase on either side amounting to a total volume V_g, the probability of insertion for an ideal gas will be 1 in the gas phase and p_{ip} in the polymer, assuming spatial invariance within the membrane itself. For N insertions, the total number of gas probes in the gas phase, n_g, will thus be

$$n_g = \frac{NV_g}{V_g + p_{ip}V_p} \tag{5}$$

n_g is directly linked to the external pressure, P, on either side of the membrane by $PV_g = n_g k_B T$, and can thus be replaced by its expression in eq 5:

$$P \approx \frac{Nk_B T}{V_g + p_{ip}V_p} \tag{6}$$

In a similar manner, the total number of gas probes inserted into the polymer, n_p, can be obtained by

$$n_p = \frac{Np_{ip}V_p}{V_g + p_{ip}V_p} \tag{7}$$

From the common denominator in eqs 6 and 7, it follows that

$$n_p \approx \frac{Pp_{ip}V_p}{k_B T} \tag{8}$$

In this work, we used the same compromise as before for the bulk;[43] i.e., 225 gas probes were inserted into the polymer matrix, which from a reverse use of eq 8 would correspond to an external pressure of 220 bar. The actual procedure for insertion has also been described earlier.[43,95] The number of gas probes to introduce into the membrane model (a total of $n_p + n_g$) was obtained under the same conditions by taking a crude estimation of the volume of the polymer, with a probability of insertion of p_{ip}, and of the volume of the free space accessible to the gas, with a probability of insertion of 1. The resulting number of gas probes was 1780,

of which half were randomly inserted in the free space on one side and the remainder into the free space on the other side of the polymer membrane.

Interestingly, Kikuchi et al.[96] have carried out nonequilibrium MD simulations of a three-phase model, referred to as a "permeation model", consisting of a rubbery matrix sandwiched between "virtual" liquid phases on either side, which maintain the polymer in place. Gas molecules, which do not interact with the virtual liquid, are then introduced on one side of the membrane.[97] In parallel, they created "sorption models", where the gas molecules were equally exposed to both sides of the polymer membrane and found analogous permeation curves for both their "permeation" and "sorption" models.[96] In the present work, since our primary interest lies in the skin effect of the membrane and gas probes do not interact with each other, averaging over penetration from both sides of the matrix seemed preferable. This is of course different from the experimental setup for permeation, which usually requires a pressure gradient in order for the transport to be monitored.[98] In a simulation, it is straightforward to know where the gas probes originate from and follow their motion. Consequently, no external pressure gradient needs to be applied.

Considering the above, it is legitimate to wonder whether Henry's law is still valid and whether gas concentration influences the permeation results. For the purpose of this paper, this is not especially relevant as the number of probes in both systems was adjusted in a consistent way. In addition, unlike slower penetrants,[95] the gas probe does not have a tendency to occupy void spaces within the matrix for a long time and "prevent" them from being accessed by other probes. As far as gas solubility is concerned, we do not expect to see a significantly different result either as, with typical bulk moduli ranging from several GPa[99] to 100 GPa for some polyimide fibers,[100] 220 bar induces a change in density which is very minor. It will be shown that Widom's insertion technique is indeed a good approximation for characterizing the solubility of the probe in the membrane and that results are consistent with Henry's law.

The production run for the bulk model was carried out over 5000 ps at constant volume. The membrane model was simulated for a longer period of 10 000 ps in order to allow for a steady-state gas concentration profile to develop. In both cases, configurations were stored at 10 ps intervals and thermodynamic and conformational data every 1 ps for postanalysis. Schematic representations of the membrane model including an interface, diffusion of the gas probes, and preferential arrangements of the polymer chains are given in Figure 2.

3. Results and Discussion

The procedure presented above is only one of many ways the glassy polyimide membrane could have been prepared. As will be shown, it leads to rather "flattened" chains throughout the whole membrane model, which obviously differ from those in the bulk. Relatively simple alternatives would have been to scale the chains centers-of-mass along the *z*-axis or to start from a preprepared bulk model in order to preserve the original structures. However, it is highly unlikely that such rigid chains would have had the possibility to relax on the MD time scale in a way consistent with the fact that polymers

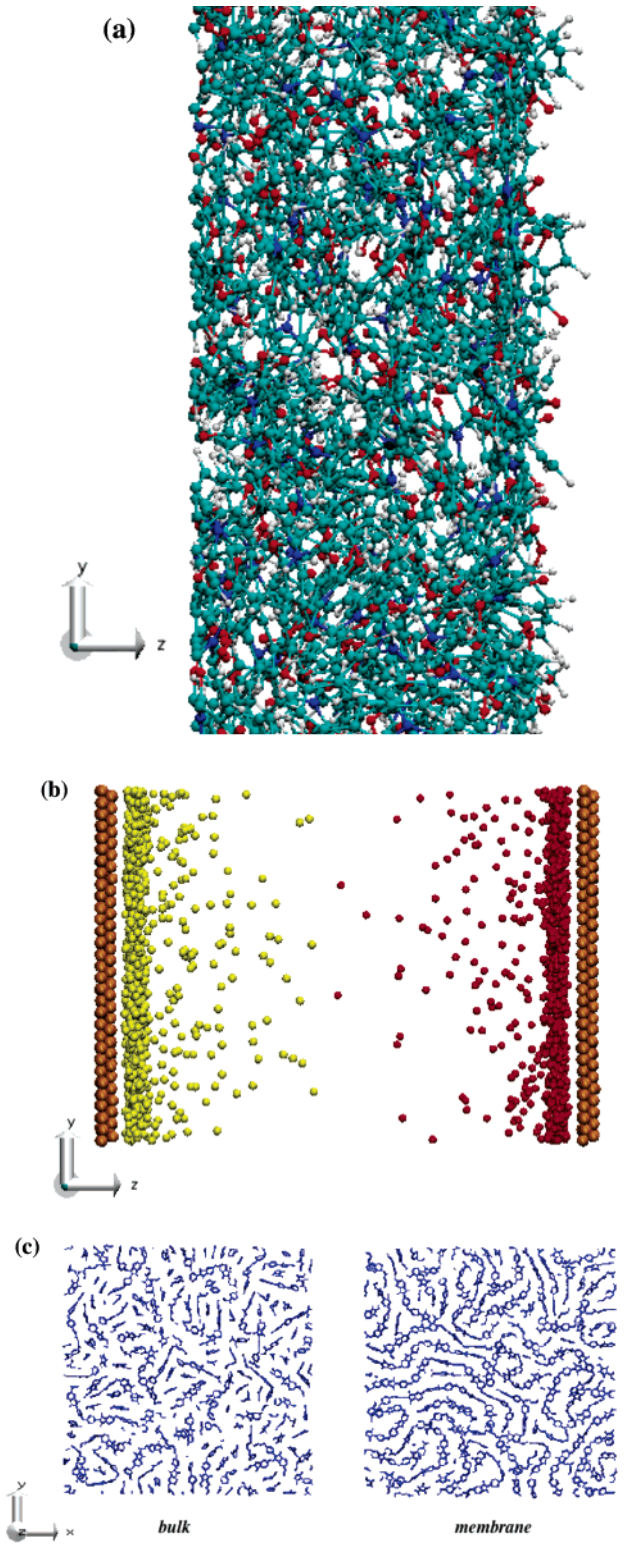

Figure 2. Schematic representations of (a) a close-up of the ODPA−ODA membrane surface on the right side (cyan = C, red = O, blue = N, white = H), with dimensions of ~32 Å along the *y*-axis and ~15 Å along the *z*-axis. (b) Gas diffusion through the membrane (snapshot at 400 ps). For clarity, gas probes have been colored in yellow (larger radii) when starting from the left and in red (smaller radii) when starting from the right. Also shown in orange is that part of the diamond-like wall which is impermeable to both polymer and gas. (c) Cross sections of width 5 Å along the *z*-axis. Only polyimides backbones are displayed. The left was taken from the middle of the bulk model while the right is the 5 Å slice of the membrane model closest to the interface. All are displayed using the VMD 1.8.2 software.[119]

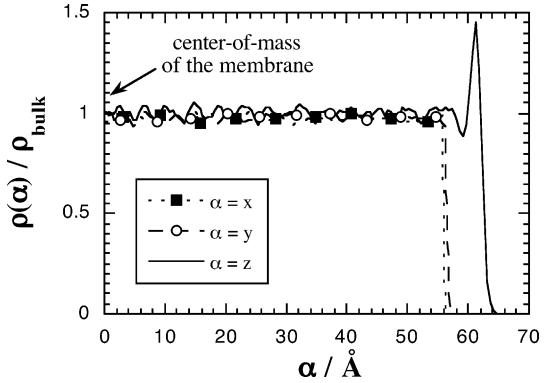

Figure 3. Mass density distributions for the polyimide atoms as a function of the distance α from the center-of-mass of the membrane along the three $\alpha = x, y$, and z directions. The $\rho(\alpha)$ curves have been symmetrized about the membrane COM and normalized with respect to the bulk model density, $\rho_{bulk} = 1378$ kg m^{-3}. The slab width is 0.5 Å.

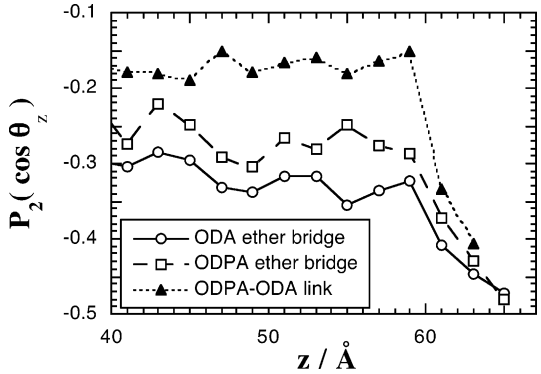

Figure 4. Average second-order Legendre polynomial functions with respect to the z axis, $P_2(\cos\theta_z)$, for pivot angles situated in slabs of width 2 Å. They are shown as a function of the z distance from the position of the pivot angle middle atom to the membrane COM. Ether bridges and ODPA−ODA links are COC and CNC angles, respectively. The curves have been symmetrized about the membrane COM, and the standard errors are smaller than the size of the symbols.

are known to form ordered and densely packed layers in contact with solid surfaces.[51,52,55,101] The same limitation would certainly occur if one was to extend the z-axis in order to eliminate interaction of the parent chains with its image in this direction as has been proposed for other more flexible polymers.[58,62,102] Although we have also recently developed a multiscale approach to that problem involving MD simulations of coarse-grained chains,[103,104] it requires a well-parametrized coarse-grain model, something which we do not have for the moment for the polyimide chains and which is well beyond the scope of the present paper. Similar approaches using reverse mapping from equilibrated coarse-grained models involving dynamic MC procedures have been reported elsewhere.[59,61] We note that this has actually been applied to three BPDA-based polyimides bulk models,[105] but it is unclear whether the obtained model densities were in agreement with the real systems.

While the question of the influence of the glassy film preparation procedure remains open, the main point of this study is to ascertain whether the interfacial structure alone *can* have an influence on gas permeation. For this purpose, we first characterize in section 3.1. in which ways the structure of our membrane model differs from that of the bulk. At later stages, we analyze whether our interfacial structure really does lead to different diffusion (section 3.2) and solubility coefficients (section 3.3).

3.1. The Membrane vs Bulk Polyimide Matrices. 3.1.1. Polymer Densities. The preparation procedure for the ODPA−ODA 56 025-atom bulk model[43] led to a density of $\rho_{bulk} = 1378$ kg m^{-3}, i.e., in excellent agreement (∼0.7%) with the experimental value of 1368 kg m^{-3}.[38] To assess the effect of the surfaces in the membrane model, the mass density distribution, $\rho(\alpha)$, of the polymer chains was calculated as a function of the distance, α, from the middle of a given slab to the center-of-mass (COM) of the membrane along the x, y, and z directions. Slabs of width 0.5 Å were chosen as a compromise between sufficient statistics and a reasonable resolution. The three $\rho(\alpha)$ functions, normalized with respect to the density of the bulk model, are displayed in Figure 3.

As expected from the preparation, the $\rho(\alpha)$ do remain very similar to ρ_{bulk} for slabs spanning the full x and y lengths of the model. It has been shown earlier[47,49−52,55,64] that the chains tend to form some densely packed layers at the vicinity of planar surfaces, which is clearly the case along the z-axis. The total length of the membrane being considered from its average limit as 65 Å on either side of its center-of-mass, the ODPA−ODA polyimides exhibit a well-defined high-density peak with a maximum situated at ∼3.5 Å and a trough at ∼6 Å from the interface. It is also possible to identify an attenuated second layer, which extends over ∼7 Å from the first peak, i.e., from ∼6 to ∼13 Å from the interface, but the remaining slab densities cannot be distinguished from ρ_{bulk}. The density is thus only perturbed on a relatively limited range at the proximity of both interfaces, in agreement with other studies.[52,55]

3.1.2. Chain Conformations and Alignments. Since polyimides such as the ODPA−ODA (Figure 1) are mostly made up of cyclic structures, their only real degrees of freedom are their "pivot angles" which correspond to the flexible ether linkages of the ODA and ODPA moieties (C−O−C bends and C−O−C−C torsions) and the more rigid ODPA−ODA linkages (C−N−C bends and C−N−C−C torsions).[40] While reliable statistics on the ⟨% trans⟩ or ⟨% gauche⟩ could not be obtained for small slab widths, the degree of alignment of the chains with respect to the interface could be characterized using the first two Legendre functions, $P_1(\cos\theta_\alpha)$ and $P_2(\cos\theta_\alpha)$, where the angle θ_α for a triplet of atoms $\{i, j, k\}$ is that between the α-axis and the vector between atoms i and k.[106]

Both Legendre functions were calculated for the pivot angles, as a function of the distance in the z direction between the middle atom (j) and the membrane COM. With a resolution of 2 Å, all $P_1(\cos\theta_z)$ remain close to zero, which shows that the results are statistically significant. The P_2 function indicates preferential alignment as its limiting values, with respect to the normal to the interface, are $-1/2$ for a perfectly perpendicular alignment, 1 for a perfectly parallel alignment, and 0 for a random alignment of the vectors defining θ_α. The average $P_2(\cos\theta_x)$, $P_2(\cos\theta_y)$, and $P_2(\cos\theta_z)$ were found to be zero for all pivot angles in the bulk model, thus confirming isotropy in that system. On the other hand, Figure 4 shows that there is a tendency along the z-axis toward perpendicular alignment of these backbone pivot angles with respect to the normal to the interface, i.e., a parallel alignment with respect to the surface and thus, by consequence, an alignment of the

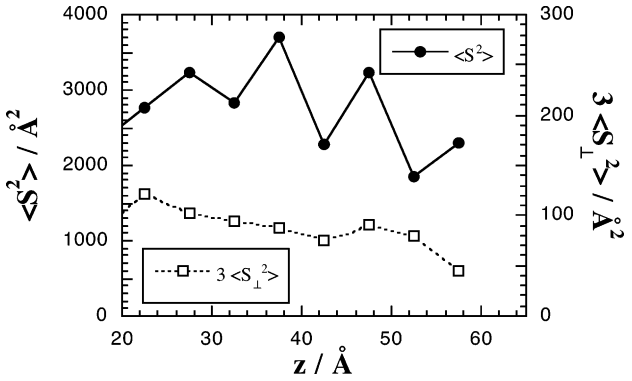

Figure 5. Mean-square radii of gyration as a function of the z distance from the chains centers of mass to the membrane COM. Note that these plots are double-Y with, on one side, the total (filled circles) and, on the other side, the component perpendicular to the membrane surface multiplied by three (open squares). The bin width is 5 Å, and the curves have been symmetrized about the membrane COM.

chains.[47,49,50,55,107] The aromatic rings align in the $x-y$ plane, which can also be seen in Figure 2c. This effect is very pronounced at the immediate vicinity of the interface, where the angles are almost perfectly parallel to the surface. However, the alignment of the chains persists into the core of the membrane, to a degree depending on the type and flexibility of the pivot angle under consideration (Figure 4). This persistence of orientation originates from the flattening induced in the chains during the compression step of the model preparation. The very low mobility of the glassy chains and the restricted amount of simulation time ensures that this feature remains throughout the whole membrane model. It should also be recalled that, despite its high cost in terms of computing power, the 141 100 atom-system "only" spans two $\langle S^2\rangle^{1/2}$ for ODPA−ODA. As far as the membrane $P_2(\cos\theta_x)$ and $P_2(\cos\theta_y)$ functions are concerned, they tend toward small positive values, typically of the order of 0.1−0.15. This is not surprising since they are inextricably linked to $P_2(\cos\theta_z)$ by the sum of the squares of the direction cosines being equal to one. The important point is though that there is no preference with respect to either x or to y. The clear alignment with respect to the z-axis is thus the main perturbation in the membrane model.

3.1.3. Chain Configurations and Structures. The polymer chain configurations were analyzed by calculating $\langle S^2\rangle$. The number of chains being relatively small (27 in the 56 025-atom bulk model vs 68 in the 141 100-atom model), the statistics are rather limited. In the bulk, $\langle S^2\rangle_{bulk}$ was found to be on average 3560 Å^2 with a standard deviation of 1340 Å^2.[43] In the case of the membrane model, $\langle S^2\rangle_{membrane} = 2760$ Å^2 with a standard deviation of 1420 Å^2. The tendency for the chains in the membrane to become flattened while they are aligned parallel to the surface is best visualized in Figure 5, which displays the histogram of $\langle S^2\rangle$ in slabs of 5 Å width accumulated according to the z distance between the chains centers-of-mass and the total membrane COM. $\langle S^2\rangle$ has also been resolved into its components perpendicular, $\langle S_\perp{}^2\rangle$, and parallel to the interface, and the former are shown in Figure 5 on a different scale. If the system was isotropic, $3\langle S_\perp{}^2\rangle$ would be equal to $\langle S^2\rangle$, which is clearly not the case. Indeed there are almost no contributions to $\langle S^2\rangle$ in the direction perpendicular to the interface, and the main components are the ones parallel to the interface. The large variations in $\langle S^2\rangle$ reflect the low number of chains contributing to a given slab, but the $\langle S_\perp{}^2\rangle$ show that the flattening effect also extends into the heart of the membrane model. It is worth noting that, in agreement with Figures 3 and 4, well-aligned chains in the immediate vicinity of the membrane are more flattened than the others. Similar results have been obtained elsewhere.[47,49−52,54]

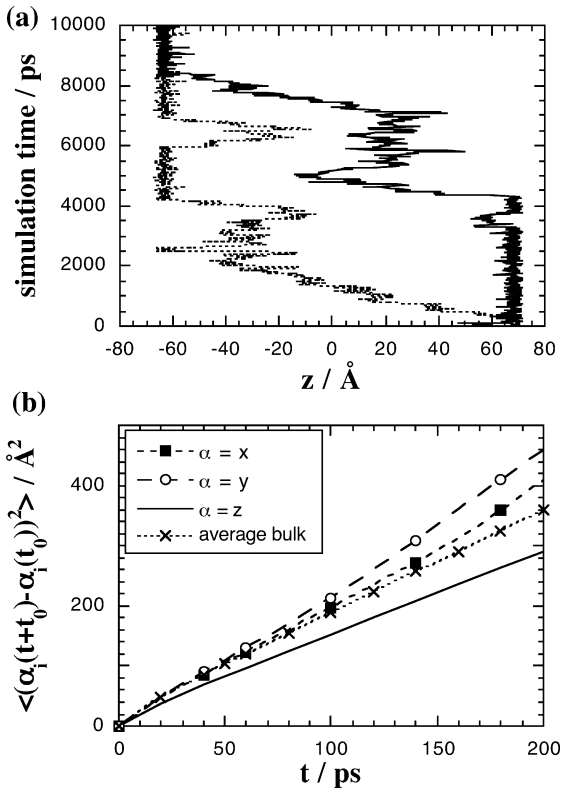

Figure 6. (a) Typical trajectories of gas probes along the z direction of the membrane model. (b) Individual x, y, and z components of the MSDs for penetrants situated in the region 10 Å to either side of the membrane COM at time t_0. The MSDs have been averaged over all possible time origins of the production run. At larger time intervals (>300 ps) the MSDs curve upward as atoms initially toward the center start to diffuse out of the membrane. The x, y, and z components of the equivalent curves in the bulk model have been averaged together since their standard deviation did not exceed 1% of their mean for a given time interval.

3.2. Diffusion in the Membrane vs the Bulk Models. 3.2.1. Individual Trajectories. The trajectories of individual gas probes were extracted from both the bulk and the membrane models. The mechanisms underlying the mobility of penetrants in polyimide bulk molecular models are now fairly well documented[18−21,43,91] and consist mainly of a succession of oscillations within available free volumes and jumping events. This type of motion is directly linked to the limited fluctuations of the glassy matrix, which allow for the temporary opening of channels and penetrant hops between different voids.[71,73,108]

A typical curve for helium diffusion through the bulk model can be found in our previous work.[43] In the present case, the use of a smaller σ for the gas probe does not qualitatively change this behavior, but the times of residence within specific holes of the polymer matrix are even more reduced and positional fluctuations are larger. This is clearly seen in Figure 6a, which displays two typical paths out of many for diffusing gas probes along the z direction of the membrane model. The probes remain for various times on either side of

the membrane but, once inside behave in very similar ways with a continuation of efficient jumps and very little time spent at a given site. The paths are not necessarily productive in terms of permeation in the sense that some probes can come back to the side of the membrane they started from.

To assess whether diffusion in the x and y direction occurs on the same extent than that in the z direction, mean-square displacements, MSDs $= \langle (r_i(t+t_0) - r_i(t_0))^2 \rangle$, were recorded as a function of time for all penetrant probes situated, at t_0, in the region 10 Å to either side of the membrane or of the bulk COM. By choosing those probes in the middle of the membrane and restricting the analysis to relatively short time intervals, the influence of those gas atoms which diffuse out of the membrane is minimized. The MSDs were then resolved into their components along the x, y, and z axes. The results are given in Figure 6b and show that diffusion is anisotropic in the membrane model, at least at short times. Indeed, the z-component of the gas MSDs is systematically lower with respect to the bulk by ~20%. On the other hand, it is compensated by an increase in both x and y components of the MSDs. Since standard deviations on the average of the x, y, and z components in the isotropic bulk are less than 1%, the differences in the components of the membrane penetrants are significant. The alignment and flattening of the chains in the anisotropic model thus leads both to a more difficult "straight" crossing of the membrane and also to a slight channeling effect along the $x-y$ plane, also visualized in Figure 2c.

3.2.2. Diffusion Coefficient in the Bulk. The most common way to obtain gas diffusion coefficients in MD simulations of bulk polymers[43] is to average the MSDs over all penetrants and over all possible time origins of the production runs, t_0. The self-diffusion coefficient D can then be evaluated using Einstein's equation,[43] which, for the present case, led to $D_{\text{bulk}} = 7.9 \times 10^{-5}$ cm^2 s^{-1}. In systems where the concentration of the diffusing species is large and penetrant−penetrant interactions cannot be overlooked, it is better to calculate instead a corrected diffusion coefficient, which accounts for the collective motion of particles under a macroscopic gradient.[109,110] However, in the present case, there are no interactions between gas probes, and D is thus a valid approximation for the true diffusivity.[73]

A second method is to accumulate the probability density distribution of displacement vector components, which can be fitted by a single Gaussian curve in the Fickian regime.[43,111] The corresponding diffusion coefficient was found to be $D_{\text{bulk}} = 8.0 \times 10^{-5}$ cm^2 s^{-1}, which is naturally in very good agreement with that evaluated using the MSDs. Finally, the consistency of these analyses was assessed using a third method, which involves calculating the self-part of the van Hove correlation function, $G_s(r,t)$.[43,112,113] We found 8.2×10^{-5} cm^2 s^{-1} for D_{bulk}, thus confirming the former results.

3.2.3. Diffusion Coefficient in the Membrane. In the membrane model, diffusion must be considered as a function of z and possibly also of the concentration of the gas at z, $c(z)$.[114] The direct resolution of the one-dimensional Fick's law diffusion equation using $D(z,c(z))$ and taking into account appropriate boundary conditions is not straightforward to fit to the obtained time- and z-dependent gas concentration.[114]

With the atomistic representation of the surface of the polyimide film used here (Figure 2a), the first problem is to define the width of the membrane, L. We used the fact that, at long times, the penetrant concentration should tend toward a constant consistent with its solubility in the membrane and the effective external pressure of the gas. Figure 7 shows a close-up in the vicinity of the interface of the symmetrized slab mass densities averaged over the last 6−10 ns of the production run for both the gas and the polyimide membrane. In this period, the gas mass density remains quasi-constant at a value of 2.84 kg m^{-3} with a standard deviation of 0.16 kg m^{-3} up to $|z| = 61.5$ Å and then increases dramatically, indicating that probes with $|z| > 61.5$ Å can be considered as belonging to the gas reservoir. As 61.5 Å also corresponds to the position of the density maximum in the first peak for the polymer membrane (Figure 7), the latter will be defined as -61.5 Å $\leq z \leq 61.5$ Å. The outside gas distribution extends up to $|z| = 70.5$ Å, i.e., for ~9 Å on either side of the membrane. In a following section we show that, despite the limited width, we just about attain ideal gas behavior at the center of this zone. In fact, extending the width of the ideal gas zone will not change the boundary conditions regarding the diffusion equation that has to be solved here and will just lead to longer calculations.

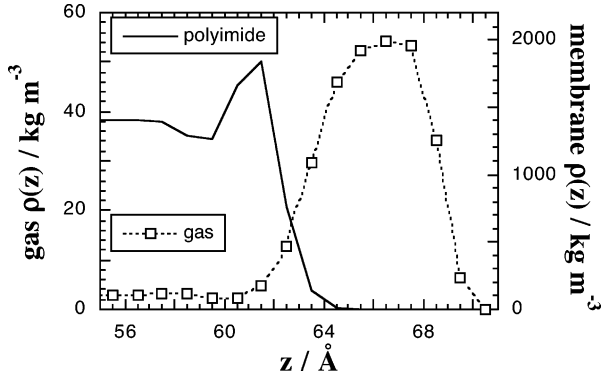

Figure 7. A close-up of the slab mass densities averaged over the 6−10 ns interval of the production run for the gas (left axis) and the polyimide (right axis) at the vicinity of the interface and as a function of the z distance from the membrane COM. The $\rho(z)$ curves have been symmetrized about the membrane COM, and the slab width is 1 Å.

The second step is to assess whether the diffusion is consistent or not with the simplest solutions of the one-dimensional diffusion equation of a substance into a permeable membrane, where D is assumed to be independent of both z and concentration, D_z. Solutions for this case are characterized[110,114] by a linear relationship between the weight gain of the polymer and $t^{1/2}$. The relative number uptake of gas probes in the membrane over the whole simulation run is presented as a function of $t^{1/2}$ in Figure 8 (solid line). In the initial 100 ps of the simulation, corresponding to the first entry of probes in the membrane, uptake scales roughly as $t^{0.35}$, but the slope found is highly dependent on the definition of the limits of the membrane. From 100 to 2000 ps, the uptake curve scales linearly as $t^{1/2}$, thus suggesting that gas diffusion is consistent with a single value of D_z in the time interval characteristic of the penetration and the motion through the membrane. After 2000 ps, gas probes have had time to diffuse through the entire membrane and start to exit in significant numbers through the second interface. At this point, the uptake curve tends toward a plateau which is attained at ~6000 ps. Of course, afterward, gas probes keep going in and

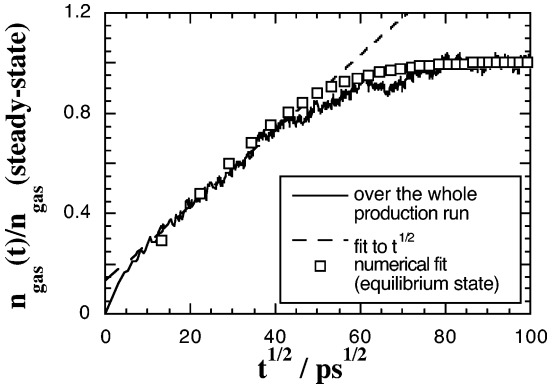

Figure 8. Relative number uptake of gas probes, defined as the number of gas probes in the membrane at time t divided by the number found in the steady-state regime, shown over the 10 000 ps of the membrane model production time (solid line). For a better identification of Fickian diffusion, the data are plotted as a function of $t^{1/2}$ along with a linear fit to $t^{1/2}$ obtained from the gas uptake over the 100−2000 ps time interval (dashed line). The squares are obtained from an appropriate numerical fit of the diffusion data in the steady state (6−10 ns), extrapolated to 10 000 ps for comparison (see text for details).

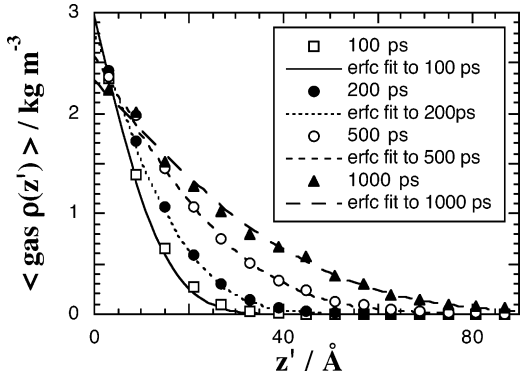

Figure 9. Mass density distributions showing the diffusion of labeled gas atoms into the membrane at time intervals of 100, 200, 500, and 1000 ps extracted from the steady-state regime (6−10 ns) of the production run. The actual profiles (displayed with symbols) have been averaged over all possible time-origins by labeling gas probes which are inside or outside of the membrane, defined by $L/2 = 61.5$ Å, at each time origin. They are shown as a function of $z' = z + (L/2)$. The slab width is 1 Å, and the profiles have been symmetrized so that molecules initially on the left side or on the right side of the membrane are considered as being equivalent. The lines are fits to the form of eq 9 with a constant diffusion coefficient of 6.8×10^{-5} cm^2 s^{-1}.

out of the membrane, but their total number within the polymer remains quasi-constant as well as the average numbers in each reservoir. This steady-state covers the 6−10 ns of the production run and is associated with the constant gas distribution displayed in Figure 7. In fact, the peak in the gas distribution between the membrane and the wall at $|z| = 66.5$ Å coincides with the point where the Widom test particle insertion probability (see later) tends to one. We can thus use the equilibrium gas density at this point to estimate the partial gas pressure using the ideal gas law, $P_{gas}V = n_{gas}kT$, which gives $P_{gas} = 340$ bar. The initial pressure at the same z and at the start of the simulation was as high as 500 bar. The equilibrium value is larger than the bulk value of 220 bar since the number of gas probes to insert into the membrane model was initially estimated assuming that the volume between the polymer and the wall would be homogeneously occupied by the penetrant. This is not the case due to the geometry and the fluctuations in the walls and in the membrane.

Up to now, we have considered the whole diffusion data taken from the start of the simulation. This nonequilibrium experiment is instructive but is expensive to repeat. We can, however, obtain similar gas concentration vs time curves from an equilibrium simulation simply by artificially labeling gas probes as being on the "left", $z_i(t_0) < -61.5$ Å, or on the "right", $z_i(t_0) > 61.5$ Å, at any particular time origin of the simulation and then subsequently following the evolution of the distribution of these t_0-labeled atoms. In this way, the time-dependent concentration profiles in the absence of any net flux can be generated by averaging over all possible time origins in the steady-state part of the simulation. As for the nonequilibrium case, the distributions for "left" and "right" molecules are subsequently symmetrized. These distributions can also be used to determine the uptake of the tagged particles into the membrane. Despite the different conditions, the equilibrium results (not shown) are superimposable with the nonequilibrium uptake curve (solid line of Figure 8) over the range of time accessible to the former. This suggests that the results are relatively insensitive to whether the membrane already contains gas probes or not. Although it is known that pressure can have effects in actual membranes depending on the diffusing molecule type,[115] the range of pressures applied here and the nature of the penetrant do not lead to any noticeable effects.

If it is assumed that, within the membrane, D_z is independent of the concentration and of the z position and that diffusion in the gas phase is considerably higher, then the following relatively simple solution for a semiinfinite system[110,114] is an instructive approximation:

$$c(z',t) = c_0 \,\mathrm{erfc}\left(\frac{z'}{\sqrt{4D_z t}}\right) \tag{9}$$

In the above equation, z' is the coordinate in a reference system where $z' = 0$ is the left edge of a membrane which extends to $z' = +\infty$. This solution is obtained given the following boundary conditions: $c(z' \geq 0, t = 0) = 0$; $c(z' = 0, t > 0) = c_0$. In our case, where the membrane is of finite length, we can define $z' = z + (L/2)$, where $L = 123$ Å is the "width" of the membrane and z is the coordinate in the frame of reference of the membrane COM; the change of variable implies that $z' = 0$ corresponds to one extremity of the membrane and $z' = L$ with the other. In addition, we have to recognize that the solution given by eq 9 is only valid up to the time when gas probes begin to cross the membrane, which happens around 2000 ps. To avoid possible artifacts due to the decreasing gas pressure on either side of the membrane (as the number of gas probes moving into the membrane is not negligible given the limited reservoir), successive slab mass density profiles for those penetrants which have entered the membrane over a time interval of t were obtained as a function of z, using only the steady-state regime of the simulation (6−10 ns), as mentioned above. They are displayed in Figure 9 along with fits to the form of eq 9 for each given time interval t. While all the fits lead to a constant diffusion coefficient of $D_z = 6.8 \times 10^{-5}$ cm^2 s^{-1}, it is clear from Figure 9 that the c_0 coefficient in eq 9 slightly decreases with increasing t. This simply shows that the

stationary source boundary condition, $c(z' = 0, t > 0) = c_0$, justifiable in the case of a constant partial pressure of the penetrant gas in the reservoir, is not consistent with the conditions used here; i.e., the partial pressure of the labeled gas probes in the (fixed volume) reservoir gradually diminishes as they diffuse into the membrane. Consequently, eq 9 cannot be considered on its own as fully appropriate for the determination of the diffusion coefficient.

To avoid the problem of the inappropriate boundary conditions associated with the analytical solutions given in eq 9, it was decided to compare the results with a numerical solution of the one-dimensional diffusion equation.[114] To do the numerical integration, the range of the membrane in the z dimension was divided into equal intervals of $\delta z = 1$ Å and the range in t into intervals of $\delta t = 0.1$ ps. Using finite difference methods, the concentration at the middle of a slab z and at time $t + \delta t$, $c(z,t+\delta t)$ can be obtained with good precision using the following algorithm:

$$c(z,t+\delta t) = c(z,t) + D_z \frac{\delta t}{\delta z^2}(c(z + \delta z, t) + c(z - \delta z, t) - 2c(z,t)) \quad (10)$$

provided that $(D_z\ \delta t/\delta z^2) < {}^1/_2$.[114] At the start of the numerical integration, the gas concentration at the left edge, z_{min}, of the membrane was set using the average gas mass density of 2.84 kg m^{-3} inside the membrane at steady state. The initial amount of gas in the reservoir to the "left" side of the membrane, $Q_L(0)$, was determined from the integral of the actual average gas distribution in the steady state (Figure 7) for $z < z_{min}$. Over the integration loop, the amount of gas either remaining in the left-side gas reservoir, $Q_L(t)$, having diffused into the membrane, $Q_M(t)$, or having exited through the right interface, $Q_R(t)$, was evaluated at each δt. These values were then used immediately to reset the imposed concentrations at the left and right edges of the membrane:

$$c(z_{min},t) = c(z_{min},0)\ Q_L(t)/Q_L(0) \quad (11a)$$

$$c(z_{max},t) = c(z_{min},0)\ Q_R(t)/Q_L(0) \quad (11b)$$

This is a reasonable approximation given that diffusion in the gas reservoirs is significantly higher than that in the membrane; i.e., it can be assumed that the gas distributions in the reservoirs are always proportional to the equilibrium one. Using this approach, the best fits to the equilibrium-determined concentration density profiles at different times were obtained with a value of $D_z = 7.5 \times 10^{-5}$ cm^2 s^{-1}. Examples of these fits are given in Figure 10. Since our specific boundary conditions are now well taken into account and the resulting diffusion coefficient is still close to that obtained from the analytical solution of eq 9, it can be safely assumed that the latter is a reasonable approximation. The nonconstant c_0 exhibited in Figure 9 is thus of little significance as far as the diffusion coefficient is concerned.

Using the best fit value for D_z of 7.5×10^{-5} cm^2 s^{-1}, the numerical integration procedure was carried out up to 10 ns so as to compare the predicted uptake of gas probes with that actually obtained using the whole production run. The numerical integration results are displayed as squares in Figure 8, and these are obviously in good agreement with the nonequilibrium experiment. This confirms the suggestion that the results are relatively insensitive to whether the membrane already contains gas probes or not.

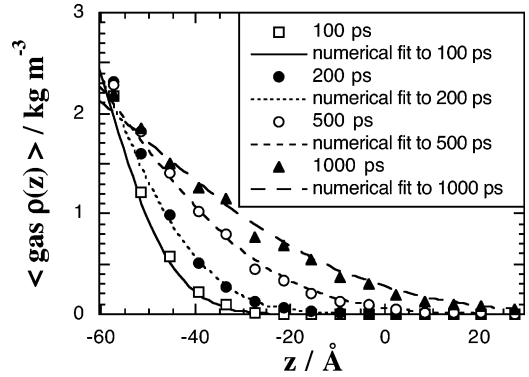

Figure 10. As Figure 9 except that the lines are now from numerical solutions of the one-dimensional diffusion equation using the algorithm given in eq 10; they are displayed as a function of the z distance and $D_z = 7.5 \times 10^{-5}$ cm^2 s^{-1}.

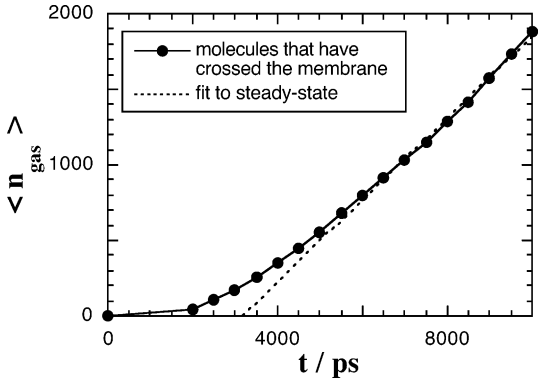

Figure 11. Average number of gas probes that at the time origin are on one side of the membrane but are to be found on the other side at a time t later. The mean has been taken over all possible time origins. The dashed line is a fit to the curve in the steady-state regime (6−10 ns), which allows the identification of the time lag as the point of intersection with the time axis.

A third way to estimate the diffusion coefficient in the membrane is to perform a time-lag analysis, analogous to what is done experimentally[98,115] by following the quantity of penetrants that have crossed the membrane after a given time interval t. The intercept on the time axis with the extrapolated linear steady-state portion of the curve is called the time lag, θ, and is directly related to the width of the membrane, L, and to the diffusion coefficient D_z by

$$D_z = \frac{L^2}{6\theta} \quad (12)$$

The resulting curve is shown in Figure 11 and shows the typical profile of a permeation experiment.[98] The intercept of the time axis with the extrapolated linear steady-state portion of the curve leads to a time lag of $\theta = 3170$ ps. It should be noted that the assumption behind eq 12 is once again that the gas pressure in the left reservoir is constant; thus, the concentration at the left interface is constant. However, we have seen that the gradually diminishing concentration at the interface does not have any significant effect on D_z. This is confirmed by the value obtained from eq 12 of $D_z = 7.9 \times 10^{-5}$ cm^2 s^{-1}, which is in very good agreement with

the diffusion coefficients obtained from both the analytic form (eq 9) and the numerical (eq 10) approach. More importantly, we do not find any notable difference with the D_{bulk}, thus showing that the diffusion coefficient is neither governed by the presence of a high-density interface nor by the changes in polyimide chain configurations and packing.

3.3. Solubility in the Membrane vs the Bulk Models. With our parameters for the gas probe, the average probability of insertion for the gas into the polymer, p_{ip}, using Widom's insertion technique[72,73] is equal to 0.055 ± 0.001, which, expressed in cm^3 (STP) cm^{-3} bar^{-1}, gives 0.049 ± 0.001, in close agreement with the experimental value for helium.[38] Widom's insertion technique was applied as well to the membrane model, and the results were analyzed as a function of the z coordinate of the test particle. A 1 Å resolution for the accumulated histogram was used, and the results were averaged over a total of 5 million insertions for each configuration taken from the last 5 ns of the production run. Insertion probabilities, $\langle p_{ip}(z) \rangle$, were also obtained independently from eq 8 since the latter can be rewritten as $p_{ip} = (n_p m_{gas}/V_p)(k_B T/P_{gas} m_{gas})$, where m_{gas} is the mass of helium, $n_p m_{gas}/V_p$ is the equilibrium density of the gas probe in the polymer, and P_{gas} is the equilibrium partial pressure of the gas in the reservoir, this latter value being taken to be 340 bar, as was estimated above. This simple alternative, which basically amounts to counting the number of gas probes inside the polymer, has been used for example in binary-phase gas/polymer models.[96,116] The results from both techniques are displayed in Figure 12a and are clearly superimposable, thus showing that Widom's insertion technique is well-suited to the estimation of gas solubility in these systems. Figure 12b shows the average equilibrium gas density in the reservoirs on either side of the membrane, along with the corresponding Widom's insertion probabilities. The latter go to 1, indicating that, despite the fairly limited size of the reservoir, an ideal gas phase is attained at the center.

It can also be seen from Figure 12 that there are no gas adsorption layers at either the polymer or wall surfaces. This could only occur if there are attractive interactions between the surfaces and the penetrant. However, as we will show in a subsequent article, even in the case of a free-standing polymer membrane in the presence of attractive potentials, this polyimide surface is actually too diffuse for a noticeable peak in $\rho_{gas}(z)$ to develop.

Despite the differences in chain configurations and alignments, the insertion probability in the center of the membrane is quasi-identical to that in the bulk. A very slight dip in solubility is found close to the interface at a point coinciding with the inner part of the high-density peak in the polymer mass distribution but is insufficient to represent any real barrier to diffusion. It should be noted that the relationship between density and solubility[117] is not very straightforward. Higher density should lead to less space available for penetrants, i.e., lower solubility. On the other hand, high density leads to higher cohesion energy density (CED), i.e., more solubility.[31] These effects could then be competing for the behavior of solubility, which include both enthalpic and entropic terms.[118] In the present model, we do not see an increase in solubility in the denser part of the membrane. To confirm that this is not an artifact due to the use of the purely repulsive WCA potential (eq 2),

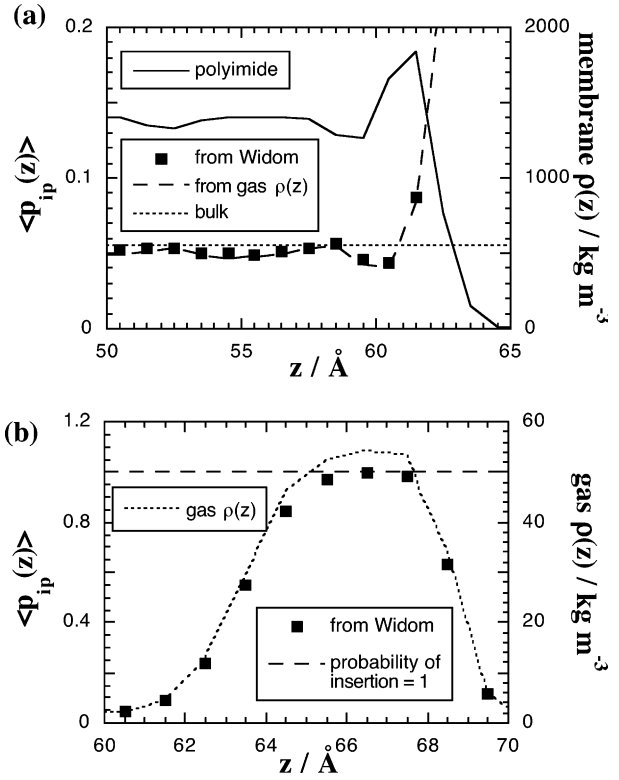

Figure 12. (a) Average probability of insertion for the gas probes into the polymer, p_{ip}, as a function of z in the steady-state regime (6−10 ns). It has been obtained both from Widom insertion's technique[72,73] (squares with a maximum standard error of 0.002) and from the equilibrium density of the gas in the polymer (long dash). $\langle p_{ip} \rangle$ in the bulk system (short dash) and the average slab mass density for the polyimide (line) are also indicated. All curves have been symmetrized about the membrane COM, and the slab width is 1 Å. (b) A close-up of the equilibrium gas density in the gas reservoir on either side of the membrane, along with the corresponding Widom's insertion probabilities. The long dashes indicate a probability of insertion of 1, i.e., an ideal gas phase.

Widom's insertion procedure was carried out in the membrane model using realistic parameters for He,[74] N_2,[42] and O_2[41] as well as the LJ form of the van der Waals potential (eq 1). The results confirmed the trend exhibited by the WCA potential, i.e., a slight decrease of solubility with increasing density. The outer part of the high-density peak corresponds to the nonsmooth polyimide surface (Figure 2a) at the contact of which the gas probes have an intermediate behavior between the gas phase and the entry into the membrane and consequently to an expected increase in solubility.

4. Conclusions

The main purpose of this study was to determine whether a "skin effect" induced by the polymer membrane preparation procedure could lead to significantly reduced gas permeation. A periodic three-dimensional representation of the amorphous core, the bulk model, was compared to a membrane model, i.e., the same polyimide confined between walls and effectively periodic in two dimensions. Despite producing a membrane with significantly oriented and flattened chains and with distinct density oscillations at the interfaces, the solubility and diffusion (and consequently the permeation) differ very little from the corresponding bulk amorphous model. In the specific case that initiated this work,[38] such skin effects are thus unlikely to explain

the discrepancies between experimental and simulated bulk diffusion coefficients.

It is important to note that these results are valid within the specific conditions of the present models and that they could be affected by a number of parameters. Indeed, we constrained the membrane model by keeping a density similar to that of the bulk in the middle of the membrane, so as to compare both models under the same density conditions. It could also be argued that the use of the purely repulsive WCA potential or that of the modified gas probe is significant. Another open question, which remains to date, is that of the preparation procedure of fully atomistic glassy models, and in the future, it would be interesting to compare it to a coarse-graining approach.[103,104] Even so, it is difficult to see how a significant reduction in diffusion and solubility could come about. One possibility might be to better take into account the solvent evaporation process. However, the influence of an ever-changing concentration on the conformational properties of the chains remains rather unknown and also difficult to incorporate a priori in any simulation given the very slow relaxation times.

This work shows clearly that aligned and flattened conformations associated with the use of a solid wall are not likely to decrease on their own the permeation parameters. We are currently studying the free-standing membrane model using the full LJ and Coulombic potentials, albeit on a much smaller time scale. In this case, there is no need to artificially constrain the polymer using walls so the density at the interface and the interior will adjust naturally to the applied gas pressure. Nevertheless, we do not anticipate that such a change will lead to a reduction in the permeability, and first indications are to the contrary.

Acknowledgment. The French IDRIS and CINES supercomputing centers are acknowledged for computer time as well as local resources at the University of Savoie (COMPAQ DS20E). The Rhône-Alpes region is thanked for funds dedicated to computer hardware and a doctoral grant for A.D.

References and Notes

(1) Ohya, H.; Kudryavtsev, V. V.; Semenova, S. I. *Polyimide Membranes—Applications, Fabrication and Properties*; Kodansha Ltd. and Gordon and Breach Science Publishers S.A.: Tokyo and Amsterdam, 1996.
(2) Paul, D. R., Yampolskii, Y. P., Eds. *Polymeric Gas Separation Membranes*; CRC Press: Boca Raton, FL, 1994.
(3) *Polyimides: Fundamentals and Applications*; Marcel Dekker: New York, 1996.
(4) Kim, T. H.; Koros, W. J.; Husk, G. R.; O'Brien, K. C. *J. Membr. Sci.* **1988**, *37*, 45.
(5) Kim, T. H.; Koros, W. J.; Husk, G. R. *Sep. Sci. Technol.* **1988**, *23*, 1611.
(6) Stern, S. A. *J. Membr. Sci.* **1994**, *94*, 1.
(7) Suzuki, T.; Yamada, Y.; Tsujita, Y. *Polymer* **2004**, *45*, 7167.
(8) Park, J. Y.; Paul, D. R. *J. Membr. Sci.* **1997**, *125*, 23.
(9) Robeson, L. M.; Smith, C. D.; Langsam, M. *J. Membr. Sci.* **1997**, *132*, 33.
(10) Yampolskii, Y.; Shishatskii, S.; Alentiev, A.; Loza, K. *J. Membr. Sci.* **1998**, *149*, 203.
(11) Thran, A.; Kroll, G.; Faupel, F. *J. Polym. Sci., Part B: Polym. Phys.* **1999**, *37*, 3344.
(12) Alentiev, A. Y.; Yampolskii, Y. P. *J. Membr. Sci.* **2000**, *165*, 201.
(13) Alentiev, A. Y.; Loza, K. A.; Yampolskii, Y. P. *J. Membr. Sci.* **2000**, *167*, 91.
(14) Ronova, I. A.; Rozhkov, E. M.; Alentiev, A. Y.; Yampolskii, Y. P. *Macromol. Theory Simul.* **2003**, *12*, 425.
(15) Allen, M. P.; Tildesley, D. J. *Computer Simulation of Liquids*; Clarendon Press: Oxford, England, 1987.
(16) Smit, E.; Mulder, M. H. V.; Smolders, C. A.; Karrenbeld, H.; Van Eerden, J.; Feil, D. *J. Membr. Sci.* **1992**, *73*, 247.
(17) Zhang, R.; Mattice, W. L. *J. Membr. Sci.* **1995**, *108*, 15.
(18) Hofmann, D.; Ulbrich, J.; Fritsch, D.; Paul, D. *Polymer* **1996**, *37*, 4773.
(19) Hofmann, D.; Fritz, L.; Ulbrich, J.; Paul, D. *Polymer* **1997**, *38*, 6145.
(20) Hofmann, D.; Fritz, L.; Ulbrich, J.; Paul, D. *Comput. Theor. Polym. Sci.* **2000**, *10*, 419.
(21) Hofmann, D.; Fritz, L.; Ulbrich, J.; Schepers, C.; Böhning, M. *Macromol. Theory Simul.* **2000**, *9*, 293.
(22) Heuchel, M.; Hofmann, D. *Desalination* **2002**, *144*, 67.
(23) Heuchel, M.; Hofmann, D.; Pullumbi, P. *Macromolecules* **2004**, *37*, 201.
(24) Pandey, P.; Chauhan, R. S. *Prog. Polym. Sci.* **2001**, *26*, 853.
(25) Pinel, E.; Barthe, M.-F.; De Baerdemaeker, J.; Mercier, R.; Neyertz, S.; Albérola, N. D.; Bas, C. *J. Polym. Sci., Part B: Polym. Phys.* **2003**, *41*, 2998.
(26) Eastmond, G. C.; Page, P. C. B.; Paprotny, J.; Richards, R. E.; Shaunak, R. *Polymer* **1993**, *34*, 667.
(27) Joly, C.; Le Cerf, D.; Chappey, C.; Langevin, D.; Muller, G. *Sep. Purif. Technol.* **1999**, *16*, 47.
(28) Kawakami, H.; Mikawa, M.; Nagaoka, S. *J. Membr. Sci.* **1996**, *118*, 223.
(29) O'Brien, K. C.; Koros, W. J.; Husk, G. R. *Polym. Eng. Sci.* **1987**, *27*, 211.
(30) Mensitieri, G.; Del Nobile, M. A.; Monetta, T.; Nicodemo, L.; Bellucci, F. *J. Membr. Sci.* **1994**, *89*, 131.
(31) Shishatskii, A. M.; Yampolskii, Y. P.; Peinemann, K.-V. *J. Membr. Sci.* **1996**, *112*, 275.
(32) Kawakami, H.; Mikawa, M.; Nagaoka, S. *J. Membr. Sci.* **1997**, *137*, 241.
(33) Kawakami, H.; Mikawa, M.; Nagaoka, S. *Macromolecules* **1998**, *31*, 6636.
(34) McCaig, M. S.; Paul, D. R. *Polymer* **2000**, *41*, 629.
(35) McCaig, M. S.; Paul, D. R.; Barlow, J. W. *Polymer* **2000**, *41*, 639.
(36) Pfromm, P. H.; Koros, W. J. *Polymer* **1995**, *36*, 2379.
(37) Huang, Y.; Paul, D. R. *Polymer* **2004**, *45*, 8377.
(38) Pinel, E. Ph.D. Thesis, University of Savoie, France, 2001.
(39) Pinel, E.; Bas, C.; Neyertz, S.; Albérola, N. D.; Petiaud, R.; Mercier, R. *Polymer* **2002**, *43*, 1983.
(40) Pinel, E.; Brown, D.; Bas, C.; Mercier, R.; Albérola, N. D.; Neyertz, S. *Macromolecules* **2002**, *35*, 10198.
(41) Fisher, J.; Lago, S. *J. Chem. Phys.* **1983**, *78*, 5750.
(42) Cheung, P. S. Y.; Powles, J. G. *Mol. Phys.* **1975**, *30*, 921.
(43) Neyertz, S.; Brown, D. *Macromolecules* **2004**, *37*, 10109.
(44) Dimitrakopoulos, C. D.; Kowalczyk, S. P. *Thin Solid Films* **1997**, *295*, 162.
(45) Frenkel, D.; Klein, M.; Parrinello, M.; Smit, B. *Understanding Molecular Simulation*, 2nd ed.; Academic Press: San Diego, CA, 2002.
(46) Madden, W. G. *J. Chem. Phys.* **1987**, *87*, 1405.
(47) Ten Brinke, G.; Ausserre, D.; Hadziioannou, G. *J. Chem. Phys.* **1988**, *89*, 4374.
(48) Kumar, S. K.; Vacatello, M.; Yoon, D. Y. *Macromolecules* **1990**, *23*, 2189.
(49) Mischler, C.; Baschnagel, J.; Binder, K. *Adv. Colloid Interface Sci.* **2001**, *94*, 197.
(50) Bitsanis, I.; Hadziioannou, G. *J. Chem. Phys.* **1990**, *92*, 3827.
(51) Vacatello, M. *Macromol. Theory Simul.* **2001**, *10*, 187.
(52) Vacatello, M. *Macromol. Theory Simul.* **2002**, *11*, 53.
(53) Vacatello, M. *Macromol. Theory Simul.* **2004**, *13*, 30.
(54) Izumisawa, S.; Jhon, M. S. *J. Chem. Phys.* **2002**, *117*, 3972.
(55) Mansfield, K. F.; Theodorou, D. N. *Macromolecules* **1991**, *24*, 4295.
(56) Schürmann, B. L.; Niebergall, U.; Severin, N.; Burger, C.; Stocker, W.; Rabe, J. P. *Polymer* **1998**, *39*, 5283.
(57) Okada, O.; Oka, K.; Kuwajima, S.; Toyoda, S.; Tanabe, K. *Comp. Theor. Polym. Sci.* **2000**, *10*, 371.
(58) Clancy, T. C.; Mattice, W. L. *Comp. Theor. Polym. Sci.* **1999**, *9*, 261.
(59) Jang, J. H.; Mattice, W. L. *Polymer* **1999**, *40*, 1911.
(60) Mansfield, K. F.; Theodorou, D. N. *Macromolecules* **1991**, *24*, 6283.
(61) Clancy, T. C.; Jang, J. H.; Dhinojwala, A.; Mattice, W. L. *J. Phys. Chem. B* **2001**, *105*, 11493.
(62) Chang, J.; Han, J.; Yang, L.; Jaffe, R. L.; Yoon, D. Y. *J. Chem. Phys.* **2001**, *115*, 2831.
(63) Van der Vegt, N. F. A.; Müller-Plathe, F.; Gelessus, A.; Johannsmann, D. *J. Chem. Phys.* **2001**, *115*, 9935.

(64) Rallabandi, P. S.; Ford, D. M. *J. Membr. Sci.* **2000**, *171*, 239.
(65) Yamamoto, H.; Mi, Y.; Stern, S. A.; St-Clair, A. K. *J. Polym. Sci., Part B: Polym. Phys.* **1990**, *28*, 2291.
(66) Jia, L.; Xu, J. *Polym. J.* **1991**, *23*, 417.
(67) Li, Y.; Ding, M.; Xu, J. *Macromol. Chem. Phys.* **1997**, *198*, 2769.
(68) Greenfield, M. L.; Theodorou, D. N. *Macromolecules* **2001**, *34*, 8541.
(69) Brown, D. *The gmq User Manual Version 3*, 1999, available at http://www.univ-savoie.fr/labos/lmops/brown/gmq.html.
(70) Brown, D.; Minoux, H.; Maigret, B. *Comput. Phys. Commun.* **1997**, *103*, 170.
(71) Gusev, A. A.; Müller-Plathe, F.; Van Gunsteren, W. F.; Suter, U. W. *Adv. Polym. Sci.* **1994**, *116*, 207.
(72) Widom, B. *J. Chem. Phys.* **1963**, *39*, 2808.
(73) Müller-Plathe, F. *Acta Polym.* **1994**, *45*, 259.
(74) Lee, J. F.; Sears, F. W.; Turcotte, D. L. *Statistical Thermodynamics,* 2nd ed.; Addison-Wesley: Reading, MA, 1973.
(75) Ewald, P. P. *Ann. Phys.* **1921**, *64*, 253.
(76) Smith, W. *Comput. Phys. Commun.* **1992**, *67*, 392.
(77) Pollock, E. L.; Glosli, J. *Comput. Phys. Commun.* **1996**, *95*, 93.
(78) Greengard, L.; Rokhlin, V. *J. Comput. Phys.* **1987**, *73*, 325.
(79) Hockney, R. W.; Eastwood, J. W. *Computer Simulation using Particles*; Institute of Physics Publishing: Bristol, UK, 1988.
(80) Darden, T.; York, D.; Pedersen, L. *J. Chem. Phys.* **1993**, *98*, 10089.
(81) York, D.; Yang, W. *J. Chem. Phys.* **1994**, *101*, 3298.
(82) Sagui, C.; Darden, T. *J. Chem. Phys.* **2001**, *114*, 6578.
(83) Beckers, J. V. L.; Lowe, C. P.; De Leeuw, S. W. *Mol. Simul.* **1998**, *20*, 369.
(84) Brandt, A. *Math. Comput.* **1977**, *31*, 333.
(85) Brown, D.; Clarke, J. H. R.; Okuda, M.; Yamazaki, T. *J. Chem. Phys.* **1994**, *100*, 1684.
(86) Brown, D.; Clarke, J. H. R.; Okuda, M.; Yamazaki, T. *J. Chem. Phys.* **1994**, *100*, 6011.
(87) Brown, D.; Clarke, J. H. R.; Okuda, M.; Yamazaki, T. *J. Chem. Phys.* **1996**, *104*, 2078.
(88) Neyertz, S.; Brown, D. *J. Chem. Phys.* **1995**, *102*, 9725.
(89) Neyertz, S.; Brown, D. *J. Chem. Phys.* **1996**, *104*, 10063.
(90) Neyertz, S.; Brown, D.; Clarke, J. H. R. *J. Chem. Phys.* **1996**, *105*, 2076.
(91) Neyertz, S.; Brown, D. *J. Chem. Phys.* **2001**, *115*, 708.
(92) Berendsen, H. J. C.; Postma, J. P. M.; Van Gunsteren, W. F.; DiNola, A.; Haak, J. R. *J. Chem. Phys.* **1984**, *81*, 3684.
(93) Koros, W. J.; Paul, D. R.; Rocha, A. A. *J. Polym. Sci., Polym. Phys. Ed.* **1976**, *14*, 687.
(94) Paul, D. R.; Koros, W. J. *J. Polym. Sci., Polym. Phys. Ed.* **1976**, *14*, 675.
(95) Neyertz, S.; Brown, D.; Douanne, A.; Bas, C.; Albérola, N. D. *J. Phys. Chem. B* **2002**, *106*, 4617.
(96) Kikuchi, H.; Fukura, M. *KGK Kautschuk Gummi Kunststoffe* **2004**, *57*, 416.
(97) Kikuchi, H.; Kuwajima, S.; Fukuda, M. *Chem. Phys. Lett.* **2002**, *358*, 466.
(98) Flaconnèche, B.; Martin, J.; Klopffer, M. H. *Oil Gas Sci. Technol.—Rev. IFP* **2001**, *56*, 245.
(99) Van Krevelen, D. W. *Properties of Polymers: their Correlation with Chemical Structure; their Numerical Estimation and Prediction from Additive Group Contributions*, 3rd completely revised ed.; Elsevier: Amsterdam, 1990.
(100) Sukhanova, T. E.; Baklagina, Y. G.; Kudryavtsev, V. V.; Maricheva, T. A.; Lednicky, F. *Polymer* **1999**, *40*, 6265.
(101) Yoon, D. Y.; Vacatello, M.; Smith, G. D. In *Monte Carlo and Molecular Dynamics Simulations in Polymer* Science; Binder, K., Ed.; Oxford University Press: New York, 1995.
(102) Natarajan, U.; Mattice, W. L. *J. Membr. Sci.* **1998**, *146*, 135.
(103) Queyroy, S. Ph.D. Thesis, University of Savoie, France, 2004.
(104) Queyroy, S.; Neyertz, S.; Brown, D.; Müller-Plathe, F. *Macromolecules* **2004**, *37*, 7338.
(105) Clancy, T. C. *Polymer* **2004**, *45*, 7001.
(106) Barbier, D.; Brown, D.; Grillet, A.-C.; Neyertz, S. *Macromolecules* **2004**, *37*, 4695.
(107) Mansfield, K. F.; Theodorou, D. N. *Macromolecules* **1990**, *23*, 4430.
(108) Gusev, A. A.; Suter, U. W.; Moll, D. J. *Macromolecules* **1995**, *28*, 2582.
(109) Tepper, H. L.; Briels, W. J. *J. Chem. Phys.* **2002**, *116*, 9464.
(110) Tsige, M.; Grest, G. S. *J. Chem. Phys.* **2004**, *120*, 2989.
(111) Neyertz, S.; Douanne, A.; Bas, C.; Albérola, N. D. *Polyimides High Perform. Polym.* **2001**, 133.
(112) Cuthbert, T. R.; Wagner, N. J.; Paulaitis, M. E.; Murgia, G.; D'Aguanno, B. *Macromolecules* **1999**, *32*, 5017.
(113) Boshoff, J. H. D.; Lobo, R. F.; Wagner, N. J. *Macromolecules* **2001**, *34*, 6107.
(114) Crank, J. C. *The Mathematics of Diffusion*, 2nd ed.; Oxford University Press: Oxford, 1979.
(115) Klopffer, M. H.; Flaconnèche, B. *Oil Gas Sci. Technol.—Rev. IFP* **2001**, *56*, 223.
(116) Kikuchi, H.; Kuwajima, S.; Fukuda, M. *J. Chem. Phys.* **2001**, *115*, 6258.
(117) Van der Vegt, N. F. A.; Briels, W. J.; Wessling, M.; Strathmann, H. *J. Chem. Phys.* **1996**, *105*, 8849.
(118) Van der Vegt, N. F. A. *J. Membr. Sci.* **2002**, *205*, 125.
(119) Humphrey, W.; Dalke, A.; Schulten, K. *J. Mol. Graph.* **1996**, *14*, 33.

MA051463Y